



OPEN ACCESS

EDITED BY

Parisa Mostafavi,
Johns Hopkins University, United States

REVIEWED BY

Laxman Adhikari,
University of Alabama in Huntsville, United States
Luca Sorriso-Valvo,
National Research Council (CNR), Italy

*CORRESPONDENCE

Andres F. Guerrero Guio,
afguerrero@unal.edu.co

RECEIVED 18 October 2023

ACCEPTED 09 January 2024

PUBLISHED 25 January 2024

CITATION

Guerrero Guio AF, Agudelo Rueda JA and Vargas Domínguez S (2024), Exploring intermittency in numerical simulations of turbulence using single and multi-spacecraft analysis.

Front. Astron. Space Sci. 11:1323993.
doi: 10.3389/fspas.2024.1323993

COPYRIGHT

© 2024 Guerrero Guio, Agudelo Rueda and Vargas Domínguez. This is an open-access article distributed under the terms of the [Creative Commons Attribution License \(CC BY\)](#). The use, distribution or reproduction in other forums is permitted, provided the original author(s) and the copyright owner(s) are credited and that the original publication in this journal is cited, in accordance with accepted academic practice. No use, distribution or reproduction is permitted which does not comply with these terms.

Exploring intermittency in numerical simulations of turbulence using single and multi-spacecraft analysis

Andres F. Guerrero Guio^{1*}, Jeffersson A. Agudelo Rueda² and Santiago Vargas Domínguez¹

¹Observatorio Astronómico Nacional, Universidad Nacional de Colombia, Bogotá, Colombia

²Department of Physics and Astronomy, Dartmouth College, Hanover, NH, United States

The energy dissipation in collisionless plasmas as the solar wind is not yet fully understood. The intermittent nature of magnetic structures appears to be a fundamental part of the energy cascade. Understanding energy transfer and dissipation in the solar wind requires an accurate description of its intermittency. Upcoming multi-spacecraft missions will provide new insight on this matter. However, the use of multi-point data requires developing new data analysis techniques as well as cross-validating these techniques. In this study, we address the latter and explore the intermittency in a 3D simulation of anisotropic plasma turbulence using two approaches. We implement the standard single-spacecraft partial variance increments technique as well as a multi-point partial variance increments technique. We contrast these two techniques and explore their dependence on the angle between the spacecraft-configuration travel direction and the background magnetic field.

KEYWORDS

plasma turbulence, intermittency, numerical simulation, multi-spacecraft analysis, HelioSwarm

1 Introduction

The solar wind, a fundamental component of our Solar System, plays a crucial role in shaping the dynamic interactions between the Sun and the surrounding space environment. This continuous stream of charged particles, primarily electrons and protons, emanates from the Sun's outermost layer, the solar corona (Gosling, 2014). Over the decades, scientific inquiry has unravelled the intricate nature of the solar wind, revealing its multifaceted impact on celestial bodies, interplanetary space, and our understanding of astrophysical phenomena. At its origin, the solar wind consists of high-energy particles with velocities exceeding 400 km per second (Marsch et al., 1982). These particles escape the Sun's gravitational pull and radiate outward in all directions, filling the entire Solar System, and becoming a prominent ingredient for the space weather. These charged particles carry with them the Sun's magnetic field, forming a complex and dynamic structure known as the interplanetary magnetic field (IMF).

The fluctuations of the magnetic field associated with charged particles are a dynamic and intriguing phenomenon and are an integral part of the interplay between the Sun and the surrounding interplanetary medium. The accurate statistical description of the magnetic field fluctuations is important because it provides valuable insights into the underlying

physical processes that govern these variations. By quantifying the statistical properties of magnetic field fluctuations, such as their amplitude, frequency, and spatial distribution, the patterns, correlations, and anomalies within the data can be discerned (Goldstein et al., 1994).

Intermittency in the solar wind refers to the phenomenon where energy at a given scale is not uniformly distributed in space (Bruno, 2019). This intermittency is linked to the non-Gaussian nature of turbulent fluctuations, with non-Gaussianity increasing at smaller scales. Instead of a uniform energy distribution, the solar wind tends to localise it in coherent structures, i.e., formations characterised by phase synchronisation across multiple scales (Perrone et al., 2017). Studying these current structures, which often give rise to what we term “coherent structures”, is directly related to energy dissipation processes typically manifesting in the so-called “energy cascades” (Dong et al., 2020). Analysing the statistics of the Probability Density Functions (PDFs) of increments provides valuable information about the distribution of coherent and intermittent structures. Notably, this method has been extensively investigated both using in-situ data and numerical simulations (Greco et al., 2009; Wu et al., 2013; Chhiber et al., 2018; Palacios et al., 2022).

It is anticipated that upcoming multi-point measurement missions, such as the Helioswarm mission (Klein et al., 2023), and mission concepts like MagneToRE (Maruca et al., 2021), will play a pivotal role in characterising current structures across various scales. Multi-spacecraft observations reveal a profound connection between space and time, as the same physical observables are measured not only at different spatial locations but also at different time instances. One of the primary challenges of multi-point measurement missions lies in reconstructing magnetic fields from data collected by distributed observatories. These innovative missions allow for diverse data analyses that enhance our understanding of turbulence and intermittency in the Earth's magnetosphere as well as in the solar wind.

Although a robust study of the intermittency involves the characterisation of the high order moments of the PDF of the increments, the Partial Variance of Increments (PVI) method (Greco et al., 2008) is a simple tool to study coherent structures using in-situ data and numerical simulations. This method involves studying magnetic field increments at different scales along a single spacecraft trajectory. The PVI method has been extended to apply to measurements taken by missions with multiple spacecraft (Chasapis et al., 2015; Yordanova et al., 2016; Pecora et al., 2023), where measurements of the magnetic field by different nodes at the same time are compared. Recent studies have analysed in-situ data from a long-duration turbulent reconnection flow in Earth's magnetotail (Chasapis et al., 2018; Huang et al., 2021). These studies are based on the analysis of statistics of magnetic field variation measured by various nodes of the MMS mission (PVI_m), and these distribution functions often follow Kappa distributions (Livadiotis and McComas, 2013).

In the present work, we study the probability distribution function (PDF) of magnetic field increments in a kinetic simulation of anisotropic plasma turbulence. We consider a single-spacecraft and a multi-spacecraft approach. We study the dependence of the PDF of the magnetic field increments on the angle between the scanning trajectory and the background magnetic field,

which aligns with the z -axis. We also explore the dependence of the PDF of the PVI as a function of the scanning angle for both the single-spacecraft case and the multi-spacecraft case. In section 2 we describe the simulation and methods that we use. In section 3 we present our results. In section 4 we discuss their implications, and finally, we conclude and suggest future work paths.

2 Methodology

In this work, we use a particle-in-cell (PIC) simulation of anisotropic Alfvénic turbulence in an ion-electron plasma in the presence of a constant background magnetic field $\mathbf{B}_0 = B_0 \mathbf{z}$ to test our methods. The simulation domain is an elongated box of size $L_x \times L_y \times L_z = 24d_i \times 24d_i \times 125d_i$ with spatial resolution $\Delta x = \Delta y = \Delta z = 0.06d_i$, where $d_i = c/\omega_{pi}$ is the ion inertial length, c is the speed of light, $\omega_{pi} = \sqrt{n_0 q_i^2 / m_i \epsilon_0}$ is the ion plasma frequency and n_0 is the constant initial ion density. For details on the simulation see (Agudelo Rueda et al., 2021).

2.1 Synthetic data

We trace synthetic trajectories across the simulation domain to collect magnetic field measurements [see Figure 1A]. In our approach, we use the Taylor hypothesis (Taylor, 1938) to treat the spatial and temporal variations interchangeably. Thus, we consider a data acquisition time $f = 15$ Hz and we assume the synthetic spacecraft sweeps the plasma with an average velocity $v_{sp} = 400$ km/s. Therefore, the resolution of our measurements and minimum lag is $\Delta s = 0.3d_i$.

In the context of pioneering multi-point missions, HelioSwarm focuses on understanding solar wind dynamics at various scales (Plice et al., 2019). This mission involves the flight of a swarm of nine satellites (1 hub and 8 nodes) to measure multiple scales simultaneously. The distance between nodes will be focused in exploring the transition region from ion kinetic scales $\gtrsim 100$ km to MHD scale $\gtrsim 1,200$ km. Although the largest size of the simulation domain is $\gtrsim 125d_i$, our results cover the small-scale range of scales be explored by Helioswarm ($\gtrsim 1 - 100 d_i$).

The regions of interest for Helioswarm include the pristine solar wind, the Earth's magnetosphere, and the magnetically connected region. In our study, we chose a spatial spacecraft configuration that corresponds to the configuration that the Helioswarm mission will display when traversing the pristine solar wind [see Figure 1B]. The positions of the nodes with respect to the hub are shown in Table 1.

2.2 Partial variance of increments for single-spacecraft

We study the variation of the magnetic field vector calculated along a one-dimensional path, represented as $\Delta \mathbf{B} = \mathbf{B}(r + \Delta s) - \mathbf{B}(r)$, where r is the position of the spacecraft and Δs represents a spatial lag in the collected data and we define the PVI index (Greco et al., 2018) as,

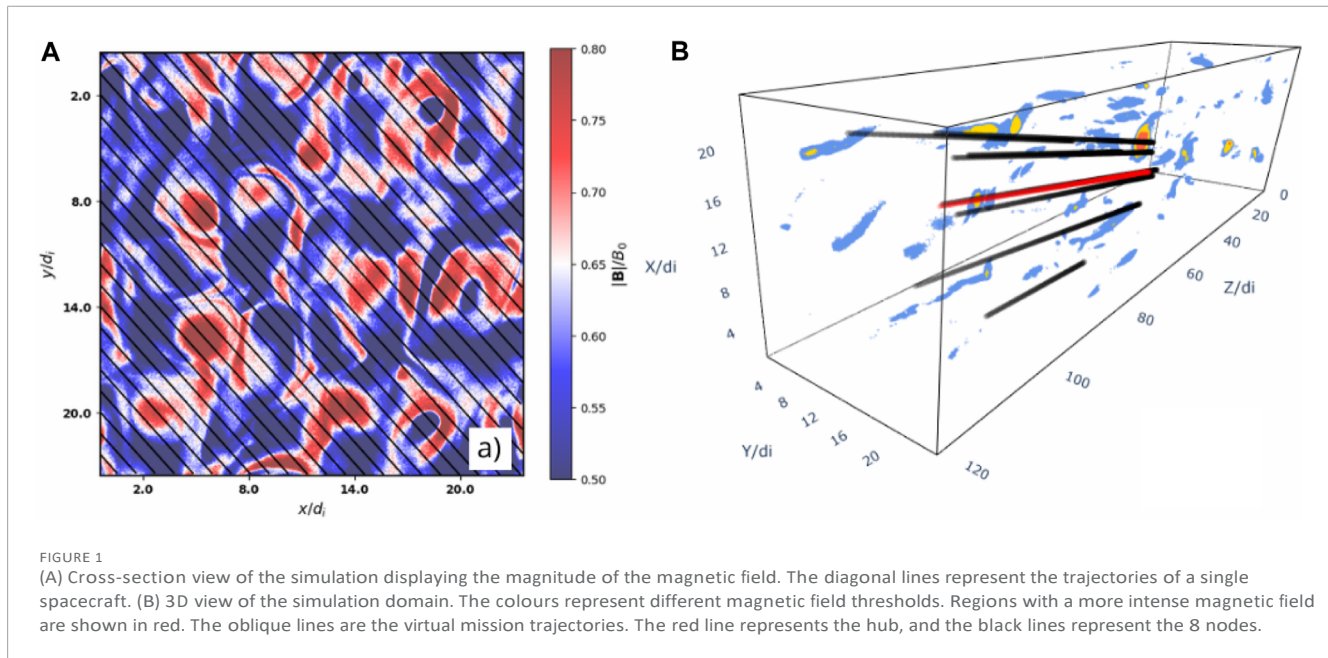


FIGURE 1

(A) Cross-section view of the simulation displaying the magnitude of the magnetic field. The diagonal lines represent the trajectories of a single spacecraft. (B) 3D view of the simulation domain. The colours represent different magnetic field thresholds. Regions with a more intense magnetic field are shown in red. The oblique lines are the virtual mission trajectories. The red line represents the hub, and the black lines represent the 8 nodes.

TABLE 1 The data represents the relative position of the HelioSwarm mission nodes in relation to the hub, expressed in units of d . The spacecraft configuration corresponds to the HelioSwarm when the mission passes through the solar wind. Retrieved from: <https://eos.unh.edu/helioswarm/multimedia>.

	$X_{GSE} [d_i]$	$Y_{GSE} [d_i]$	$Z_{GSE} [d_i]$
hub	0.00	0.00	0.00
node 1	1.31	2.73	3.61
node 2	5.98	-5.45	7.19
node 3	-10.21	3.45	-4.16
node 4	1.95	-4.55	-11.71
node 5	-2.48	5.75	11.42
node 6	3.50	-0.39	-2.58
node 7	6.03	0.40	1.78
node 8	-0.60	1.40	0.77

$$PVI = \frac{|\Delta B(r, \Delta s)|}{\sqrt{\langle |\Delta B(r, \Delta s)|^2 \rangle}} \quad (1)$$

here $\langle \dots \rangle$ represents the average over a sufficiently large interval. In our context, we apply this averaging process to all the data points within a trajectory. First, we investigate the behaviour of ΔB in a two-dimensional section of the simulation perpendicular to the background magnetic field $B_0 z$. To do this, we take a cross-section slice in the xy -plane at $z/d_i = 63.9$ and we consider multiple trajectories on this plane resembling multiple crossings of a single spacecraft through the plasma, shown in Figure 1A). We also study

the distribution of magnetic field increments when considering 3D trajectories across the entire simulation domain.

2.3 Partial variance of increments multi-spacecraft

We analyse the PDFs of ΔB for the data collected by the multi-spacecraft configuration. This is done using the aforementioned frequency and flow velocity. The analysis of the multi-point data is being carried out by comparing measurements taken by each pair of nodes at the same time. We examined the multi-point magnetic field variance, denoted as $\Delta B_{ij}(r) = B^i(r) - B^j(r)$, where i and j represent individual nodes or hub, ranging from $i, j = 1, 2, 3, \dots, 9$, with $i \neq j$. Thus, we define the PVI multi-spacecraft index as:

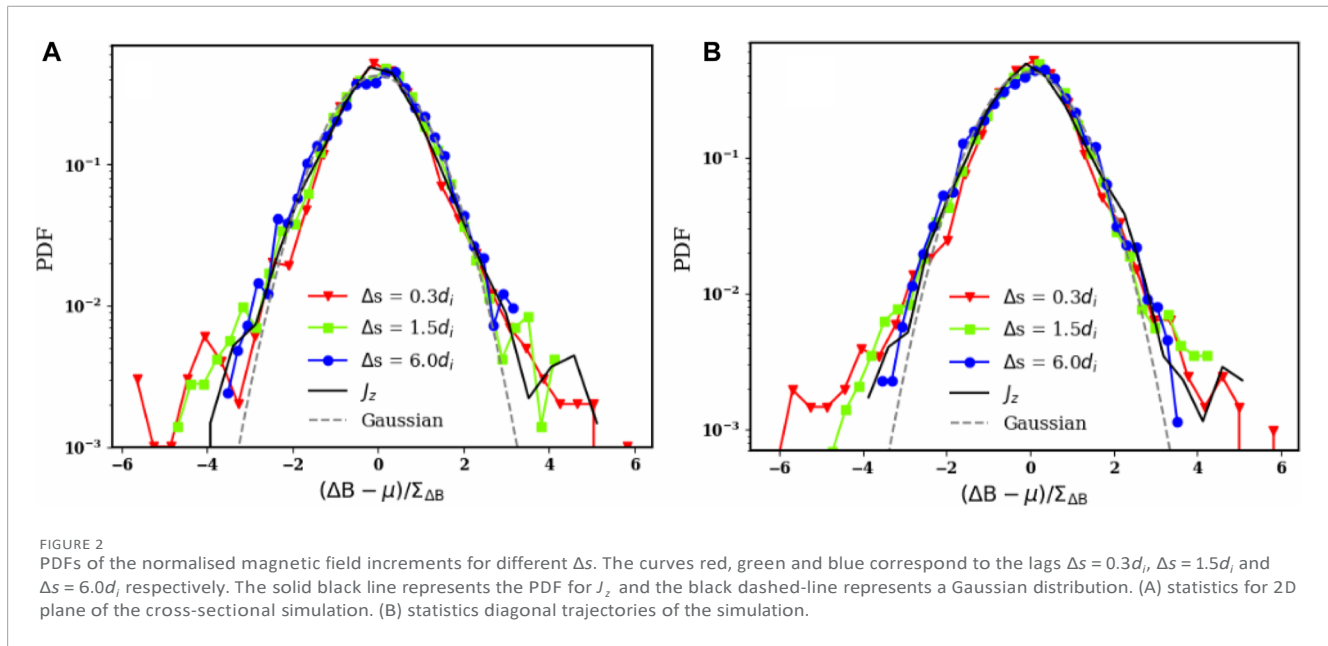
$$PVI_m^{ij} = \sqrt{\frac{|\Delta B_{ij}(t)|^2}{\langle |\Delta B_{ij}(t)|^2 \rangle_m}} \quad (2)$$

where $\langle \dots \rangle_m$ represents the average over the different pair of spacecraft. Notably, the term s that appears in “single-spacecraft” is omitted. This omission is attributed to the fact that the sampling lag is inherently determined by the distances between the pairs of spacecraft being sampled. Thus, this method enables a multi-scale analysis, driven by the varying distances between the spacecraft configured within the mission.

3 Results

3.1 Analysis of the PDF of the magnetic field increments for single-spacecraft and multi-spacecraft

In Figure 2, we present the Probability Density Functions of the magnetic field increment values. The argument of each



PDF is normalised in each case by its standard deviation $\Sigma_{\Delta B} = \sqrt{\sum (\Delta B - \mu)^2 / L}$, where L is the total number of data points and $\mu = \sum \Delta B / L$ is the mean value. The colours distinguish various lags used in computing the PVI index method, with $\Delta s = 0.3d_i$. The shortest lag (smaller scales) is denoted by red, $\Delta s = 1.5d_i$ by green, and $6.0d_i$ (the longest lag representing larger scales) is shown in blue. The solid black line represents the PDF corresponding to the z-component of the current density, while the dashed line represents the Gaussian fit applied to the values of the current density.

Figure 2A, we display the statistics corresponding to the trajectories in the 2D plane of the cross-sectional simulation. On the other hand, in Figure 2B, we present the statistics corresponding to the diagonal trajectories of the simulation.

We observe a deviation from the reference Gaussian when $|(\Delta B - \mu)/\Sigma_{\Delta B}| > 2.5$ for all lags considered in both case studies. Notably, a more distinct deviation from the Gaussian reference is evident for shorter lags, while longer lags ($\Delta s = 6.0d_i$, depicted in blue) show a closer resemblance to the Gaussian distribution. Specifically, the PDF for $\Delta s = 0.3d_i$ exhibits heavy-tailed distributions compared to the case with $\Delta s = 6.0d_i$. It is worth mentioning that no noticeable distinction is apparent between the plots obtained for different mission sweeps.

3.2 Dependence of the PDF of the magnetic field increments on the scanning angle

To study the dependence of the PDF of the magnetic field increments on the scanning angle with respect to the background magnetic field, we compute the angle between the line connecting the spacecrafts i and j and the background magnetic field B_0 as

$$\tan \theta_{ij,BO} = \frac{\rho_{ij}}{\Delta z_{ij}}, \quad (3)$$

where $\Delta z_{ij} = z_i - z_j$ is the component of the distance parallel to z and $\rho_{ij} = \sqrt{(x_i - x_j)^2 + (y_i - y_j)^2}$ is the distance perpendicular to z . Moreover, to enhance the data sample we add four additional angles $\theta_t = \pi/6, \pi/4, \pi/3, \pi/2$ between the spacecraft configuration and z , Eq. 1 and compute

$$\theta = \theta_t + \theta_{ij,BO}. \quad (4)$$

Thus, we consider 180 different distributions of increments $f_{\Delta B,ij}(\Delta s_{ij}, \theta)$. For each distribution, there is a lag Δs_{ij} associated with the separation of a pair of spacecrafts and a given angle θ . To estimate the level of intermittency, we sample the distribution $f_{\Delta B,ij}$ using $N = 40$ bins. For each bin N in the distribution we compute the difference $f_{\Delta B,ij} - f_0$ between the distribution $f_{\Delta B,ij}$ and a standard normal distribution $f_0 = e^{-(\Delta B)^2/2\pi}$. Thus, we define the distance

$$D_{ij} = \langle |f_{\Delta B,ij} - f_0| \rangle_N \quad (5)$$

where $\langle \dots \rangle_N$ is the average over the total number of bins.

Figure 3A), presents the PDFs of magnetic field increment values obtained from measurements by a single-spacecraft. In this particular case, we have employed a constant lag $\Delta s = 0.6d_i$. The colour scheme in this Figure corresponds to the variation of angle within the trajectory concerning the z -axis, with sweep angles depicted as follows: 0 in black, $\pi/6$ in red, $\pi/4$ in blue, $\pi/3$ in green, and finally, $\pi/2$ in yellow. The dashed-line represents a Gaussian distribution for reference. For all angles, the PDF of the magnetic field increments shows a distinct deviation from the reference Gaussian at ± 2.5 . For this lag, there is no clear dependence of the PDF of the increments on the scanning angle.

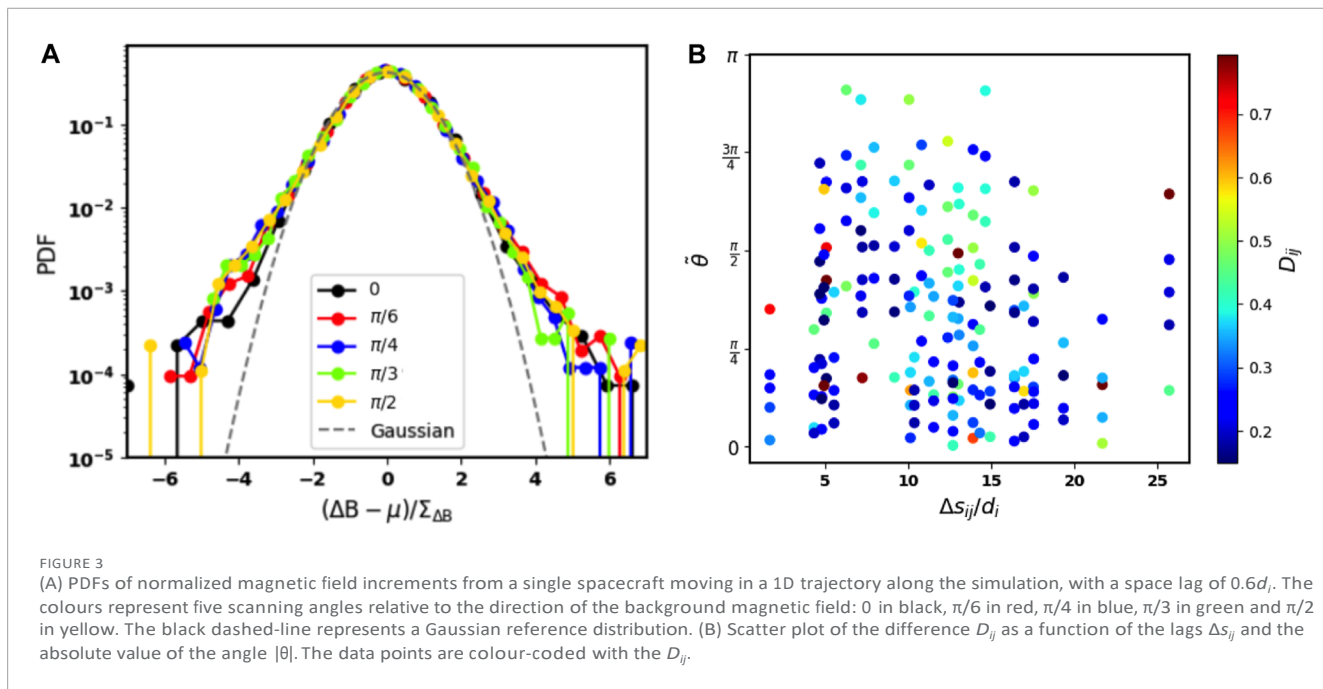


FIGURE 3
(A) PDFs of normalized magnetic field increments from a single spacecraft moving in a 1D trajectory along the simulation, with a space lag of $0.6d_i$. The colours represent five scanning angles relative to the direction of the background magnetic field: 0 in black, $\pi/6$ in red, $\pi/4$ in blue, $\pi/3$ in green and $\pi/2$ in yellow. The black dashed-line represents a Gaussian reference distribution. (B) Scatter plot of the difference D_{ij} as a function of the lags Δs_{ij} and the absolute value of the angle $|\theta|$. The data points are colour-coded with the D_{ij} .

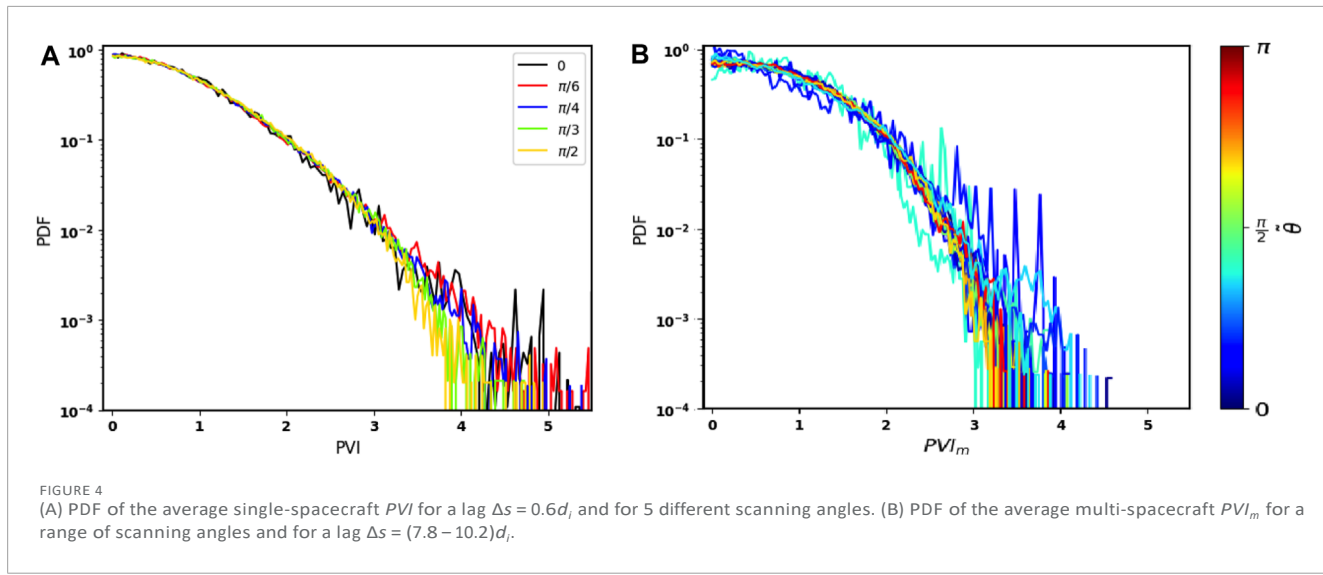


FIGURE 4
(A) PDF of the average single-spacecraft PVI for a lag $\Delta s = 0.6d_i$ and for 5 different scanning angles. (B) PDF of the average multi-spacecraft PVI_m for a range of scanning angles and for a lag $\Delta s = (7.8 - 10.2)d_i$.

Figure 3B shows a scatter plot of D_{ij} as a function of the lags Δs_{ij} and the absolute value of the angle $|\theta|$, Eq. 2. The data points are colour-coded Eq. 3 from small (blue) to large (red) D_{ij} . This plot shows that the data points are broadly distributed in both Δs_{ij} and $|\theta|$. There is no clear correlation between D_{ij} and Δs_{ij} . Since the minimum distance between a pair of spacecrafts corresponds to a lag $\Delta s_{ij} = 1.71d_i$, the PDF of the magnetic increments is not expected to deviate from the Gaussian of reference, therefore the distance is $D_{ij} < 1$ is small.

In Figure 3B there is no clear correlation between D_{ij} and $|\theta|$ which shows that there is no preferential direction parallel or perpendicular with respect to the background magnetic field.

Figure 4A depicts the Probability Distribution Function of the average single-spacecraft PVI index, Eq. 4 for five scanning angles

and for a lag $\Delta s = 0.6d_i$. In this representation, the colours indicate the scanning angle of the multi-spacecraft mission relative to the z-axis, with scanning angles ranging from 0 to $\pi/2$. The distribution follows a decreasing trend and exhibits large values for low PVI thresholds. Additionally, a steeper decline is observed for PVI values exceeding 1.8. There is no clear dependence of the PDF of the single-spacecraft PVI as a function of the scanning angle for $PVI < 3$. Only at $PVI > 3$ the larger the angle, the steeper the PDF of the PVI is. However, the statistical noise is dominant for $PVI > 4$.

Figure 4B shows the Probability Distribution Function of the average multi-spacecraft PVI_m index, Eq. 5, for a range of scanning angles and for a lag $\Delta s = (7.8 - 10.2)d_i$. For this case, the PDF of PVI_m at small angles $\theta < \pi/2$ show large

noise. The PDF of PVI_m shows no clear dependence with the scanning angle. Compared to the single-spacecraft PVI, the PDF of the PVI_m does not show a sustained slope. In contrast, the PDF of PVI_m decades rapidly into the range $3 < PVI_m < 4$. The difference is due to the larger lag compared to the single-spacecraft case.

4 Discussion and conclusion

Figure 2 indicate a transition from a Gaussian distribution at larger scales $\Delta s = 6.0d_i$ to a non-Gaussian distribution with heavy tails at smaller scales $\Delta s = 0.3d_i$. This phenomenon has already been reported in previous studies (Sorriso-Valvo et al., 1999).

Although we do not use 2D simulations, we study the 2D character of the intermittency in our simulation by taking trajectories along the plane perpendicular to the background magnetic field. Previous studies show a difference between the distribution of the increments in the 2D case compared to the 3D case (Greco et al., 2009). However, we observe no difference between the distributions for 2D trajectories and 3D trajectories crossing the entire simulation domain. This as result of the large amplitude of magnetic fluctuations in the simulation.

In Figure 3 the distributions estimated using the multi-point approach exhibit a behaviour closer to a Gaussian distribution with no tails. Moreover, the multi-point approach underestimates the level of intermittency with respect to the single-point approach. This is due to the minimum distance in the multi-spacecraft approach is larger than the scales at which the deviation from the Gaussian occurs for the single-spacecraft approach. As detailed in Table 1, the lag values that we use to sample the data in our multi-point approach span from 1.7 to 25.7 d_i , with an average of 11.7 d_i . These scales are significantly larger than those sampled in the one-dimensional approach for which the non-Gaussian features show up. Thus, this approach only considers large scales, as illustrated in Figure 2, and enforces a minimum lag limited by the spacecraft separation when investigating intermittency.

The PDFs of the PVI_m multi-spacecraft (Figure 4B) follow the shape of the decreasing exponential distribution. This result aligns with previous observational and simulation studies regarding the distribution of the multi-point PVI index, with the so-called kappa distribution (Chasapis et al., 2018; Pollock et al., 2018; Huang et al., 2021). However, for lower PVI values, we observe higher probabilities and a shift in the distribution's peak compared to previous studies.

The spacecraft separation for the MMS mission is $\approx d_i$, hence the effect of the intermittency is clear in the distribution of PVI_m (Chasapis et al., 2018) as well as in the distribution of the PVI for the single spacecraft, (Figure 4A). In our case, for the distribution of PVI_m , since the spacecraft separation is $\approx 10d_i$ the intermittency feature is less clear. Nevertheless, our results show no clear dependence with the scanning angle. This is due to the large amplitude of the magnetic fluctuations in the simulation ($\delta B \approx B_0$). This is not the case for the solar wind, where the amplitude of the magnetic fluctuations varies [$0.1 \leq \delta B \leq B_0$] and can also change as a function of heliospheric

distance (Šafránková et al., 2023). Since the solar wind conditions vary depending on its origin, velocity and heliospheric distance, our results are mainly relevant to the solar wind conditions at heliospheric distances at which $\beta \approx 1$ and populated by Alfvénic fluctuations as well as in the magnetosheath for intervals where $\beta \approx 1$. Thus, our results can be used to study the turbulence present in the solar wind and the magnetosheath provided a data discrimination of the multi-point mission data based on the solar wind velocity. This can be applied to the upcoming Helioswarm mission.

Finally, our results contribute to the state of art multi-point analysis techniques (Broeren et al., 2021; Maruca et al., 2021; Pecora et al., 2023) and are highly relevant to the development and implementation of multi-point techniques, particularly for missions with more than 4-spacecraft in which data rapidly becomes complex and difficult to handle.

Data availability statement

Publicly available datasets were analyzed in this study. This data can be found here: <https://zenodo.org/records/4313310> Three-dimensional magnetic reconnection in particle-in-cell simulations of anisotropic plasma turbulence (Simulation Data).

Author contributions

AG: Conceptualization, Data curation, Formal Analysis, Investigation, Methodology, Writing—original draft. JA: Conceptualization, Data curation, Formal Analysis, Investigation, Methodology, Writing—original draft. SV: Conceptualization, Data curation, Formal Analysis, Investigation, Methodology, Writing—original draft.

Funding

The author(s) declare financial support was received for the research, authorship, and/or publication of this article. JA is supported by NASA grant 80NSSC21K2048 and NSF grant 2142430.

Acknowledgments

We acknowledge the Beyond Research program from Facultad de Ciencias, Universidad Nacional de Colombia.

Conflict of interest

The authors declare that the research was conducted in the absence of any commercial or financial relationships that could be construed as a potential conflict of interest.

Publisher's note

All claims expressed in this article are solely those of the authors and do not necessarily represent those of their affiliated

organizations, or those of the publisher, the editors and the reviewers. Any product that may be evaluated in this article, or claim that may be made by its manufacturer, is not guaranteed or endorsed by the publisher.

References

Agudelo Rueda, J. A., Verscharen, D., Wicks, R. T., Owen, C. J., Nicolaou, G., Walsh, A. P., et al. (2021). Three-dimensional magnetic reconnection in particle-in-cell simulations of anisotropic plasma turbulence. *J. Plasma Phys.* 87, 905870228. doi:10.1017/s0022377821000404

Broeren, T., Klein, K., TenBarge, J., Dors, I., Roberts, O., and Verscharen, D. (2021). Magnetic field reconstruction for a realistic multi-point, multi-scale spacecraft observatory. *Front. Astronomy Space Sci.* 8, 727076. doi:10.3389/fspas.2021.727076

Bruno, R. (2019). Intermittency in solar wind turbulence from fluid to kinetic scales. *Earth Space Sci.* 6, 656–672. doi:10.1029/2018EA000535

Chasapis, A., Matthaeus, W. H., Parashar, T. N., Wan, M., Haggerty, C. C., Pollock, C. J., et al. (2018). In situ observation of intermittent dissipation at kinetic scales in the earth's magnetosheath. *Astrophysical J. Lett.* 856, L19. doi:10.3847/2041-8213/aaadf8

Chasapis, A., Retinò, A., Sahraoui, F., Canu, P., Vaivads, A., Khotyaintsev, Y. V., et al. (2015). Thin current sheets and associated electron heating in turbulent space plasma. *Astrophysical J. Lett.* 804, L1. doi:10.1088/2041-8205/804/1/L1

Chhiber, R., Chasapis, A., Bandyopadhyay, R., Parashar, T., Matthaeus, W. H., Maruca, B., et al. (2018). Higher-order turbulence statistics in the earth's magnetosheath and the solar wind using magnetospheric multiscale observations. *J. Geophys. Res. Space Phys.* 123, 9941–9954. doi:10.1029/2018ja025768

Dong, S., Huang, Y., Yuan, X., and Lozano-Durán, A. (2020). The coherent structure of the kinetic energy transfer in shear turbulence.

Goldstein, M., Roberts, D., and Fitch, C. (1994). Properties of the fluctuating magnetic helicity in the inertial and dissipation ranges of solar wind turbulence. *J. Geophys. Res. Space Phys.* 99, 11519–11538. doi:10.1029/94ja00789

Gosling, J. T. (2014). "The solar wind," in Encyclopedia of the solar system (Elsevier), 261–279.

Greco, A., Chuychai, P., Matthaeus, W. H., Servidio, S., and Dmitruk, P. (2008). Intermittent mhd structures and classical discontinuities. *Geophys. Res. Lett.* 35. doi:10.1029/2008GL035454

Greco, A., Matthaeus, W. H., Perri, S., Osman, K. T., Servidio, S., Wan, M., et al. (2018). Partial variance of increments method in solar wind observations and plasma simulations. *Wind Observations Plasma Simulations* 214, 1. doi:10.1007/s11214-017-0435-8

Greco, A., Matthaeus, W. H., Servidio, S., Chuychai, P., and Dmitruk, P. (2009). Statistical analysis of discontinuities in solar wind ace data and comparison with intermittent mhd turbulence. *Astrophysical J.* 691, L111–L114. doi:10.1088/0004-637X/691/2/L111

Huang, S., Zhang, J., Yuan, Z., Jiang, K., Wei, Y., Xu, S., et al. (2021). Intermittent dissipation at kinetic scales in the turbulent reconnection outflow. *Geophys. Res. Lett.* 49. doi:10.1029/2021GL096403

Klein, K. G., Spence, H., Alexandrova, O., Argall, M., Arzamasskiy, L., Bookbinder, J., et al. (2023). Helioswarm: a multipoint, multiscale mission to characterize turbulence. arXiv preprint arXiv:2306.06537.

Livadiotis, G., and McComas, D. (2013). Understanding kappa distributions: a toolbox for space science and astrophysics. *Space Sci. Rev.* 175, 183–214. doi:10.1007/s11214-013-9982-9

Marsch, E., Mühlhäuser, K.-H., Schwenn, R., Rosenbauer, H., Pilipp, W., and Neubauer, F. (1982). Solar wind protons: Three-dimensional velocity distributions and derived plasma parameters measured between 0.3 and 1 au. *J. Geophys. Res. Space Phys.* 87, 52–72. doi:10.1029/ja087ia01p00052

Maruca, B. A., Agudelo Rueda, J. A., Bandyopadhyay, R., Bianco, F. B., Chasapis, A., Chhiber, R., et al. (2021). Magnetore: mapping the 3-d magnetic structure of the solar wind using a large constellation of nanosatellites. *Front. astronomy space Sci.* 8, 665885. doi:10.3389/fspas.2021.665885

Palacios, J. C., Bourouaine, S., and Perez, J. C. (2022). On the statistics of elssasser increments in solar wind and magnetohydrodynamic turbulence. *Astrophysical J. Lett.* 940, L20. doi:10.3847/2041-8213/ac92f6

Pecora, F., Servidio, S., Primavera, L., Greco, A., Yang, Y., and Matthaeus, W. H. (2023). Multipoint turbulence analysis with helioswarm. *Astrophysical J. Lett.* 945, L20. doi:10.3847/2041-8213/acbb03

Perrone, D., Alexandrova, O., Roberts, O. W., Lion, S., Lacombe, C., Walsh, A., et al. (2017). Coherent structures at ion scales in fast solar wind: cluster observations. *Astrophysical J.* 849, 49. doi:10.3847/1538-4357/aa9022

Plice, L., Perez, A. D., and West, S. (2019). Helioswarm: swarm mission design in high altitude orbit for heliophysics.

Pollock, C., Burch, J., Chasapis, A., Giles, B., Mackler, D., Matthaeus, W., et al. (2018). Magnetospheric multiscale observations of turbulent magnetic and electron velocity fluctuations in earth's magnetosheath downstream of a quasi-parallel bow shock. *J. Atmos. Solar-Terrestrial Phys.* 177, 84–91. doi:10.1016/j.jastp.2017.12.006

Sáfránková, J., Němeček, Z., Němc, F., Verscharen, D., Horbury, T. S., Bale, S. D., et al. (2023). Evolution of magnetic field fluctuations and their spectral properties within the heliosphere: statistical approach. *Astrophysical J. Lett.* 946, L44. doi:10.3847/2041-8213/accc531

Sorriso-Valvo, L., Carbone, V., Veltri, P., Consolini, G., and Bruno, R. (1999). Intermittency in the solar wind turbulence through probability distribution functions of fluctuations. *Geophys. Res. Lett.* 26, 1801–1804. doi:10.1029/1999GL900270

Taylor, G. I. (1938). The spectrum of turbulence. *Proc. R. Soc. Lond. Ser. A-Mathematical Phys. Sci.* 164, 476–490. doi:10.1098/rspa.1938.0032

Wang, X., Tu, C., and He, J. (2020). Fluctuation amplitudes of magnetic-field directional turnings and magnetic-velocity alignment structures in the solar wind. *Astrophysical J.* 903, 72. doi:10.3847/1538-4357/abb883

Wu, P., Perri, S., Osman, K., Wan, M., Matthaeus, W., Shay, M., et al. (2013). Intermittent heating in solar wind and kinetic simulations. *Astrophysical J. Lett.* 763, L30. doi:10.1088/2041-8205/763/2/L30

Yordanova, E., Vörös, Z., Varsani, A., Graham, D. B., Norgren, C., Khotyaintsev, Y. V., et al. (2016). Electron scale structures and magnetic reconnection signatures in the turbulent magnetosheath. *Geophys. Res. Lett.* 43, 5969–5978. doi:10.1002/2016gl069191